Journal of Photochemistry & Photobiology, B: Biology 258 (2024) 112986

Contents lists available at ScienceDirect

Journal of Photochemistry & Photobiology, B: Biology

journal homepage: www.elsevier.com/locate/jphotobiol

Dynamic insights into mitochondrial function: Monitoring viscosity and SO_2 levels in living cells

Dilka Liyana Arachchige [a,b], Sushil K. Dwivedi [a,b,*], Adenike Mary Olowolagba [a,b], Joseph Peters [a,b], Ashlyn Colleen Beatty [c], Alicia Guo [e], Crystal Wang [d], Thomas Werner [c], Rudy L. Luck [a,*], Haiying Liu [a,b,*]

[a] Department of Chemistry, Michigan Technological University, Houghton, MI 49931, United States of America
[b] Health Research Institute, Michigan Technological University, Houghton, MI 49931, United States of America
[c] Department of Biological Sciences, Michigan Technological University, Houghton, MI 49931, United States of America
[d] Houghton High School, 1603 Gundlach Rd, Houghton, MI 49931, United States of America
[e] Trinity School at River Ridge/Eagan, St Paul, MN 55121, United States of America

ARTICLE INFO

Keywords:
Viscosity
Cell imaging
Ratiometric fluorescent probe
Sulfur dioxide (SO_2)
Mitochondria
Drosophila melanogaster larvae

ABSTRACT

Mitochondria, central organelles pivotal for eukaryotic cell function, extend their influence beyond ATP production, encompassing roles in apoptosis, calcium signaling, and biosynthesis. Recent studies spotlight two emerging determinants of mitochondrial functionality: intramitochondrial viscosity and sulfur dioxide (SO_2) levels. While optimal mitochondrial viscosity governs molecular diffusion and vital processes like oxidative phosphorylation, aberrations are linked with neurodegenerative conditions, diabetes, and cancer. Similarly, SO_2, a gaseous signaling molecule, modulates energy pathways and oxidative stress responses; however, imbalances lead to cytotoxic sulfite and bisulfite accumulation, triggering disorders such as cancer and cardiovascular anomalies. Our research focused on development of a dual-channel fluorescent probe, applying electron-withdrawing acceptors within a coumarin dye matrix, facilitating monitoring of mitochondrial viscosity and SO_2 in live cells. This probe distinguishes fluorescence peaks at 650 nm and 558 nm, allowing ratiometric quantification of SO_2 without interference from other sulfur species. Moreover, it enables near-infrared viscosity determination, particularly within mitochondria. The investigation employed theoretical calculations utilizing Density Functional Theory (DFT) methods to ascertain molecular geometries and calculate rotational energies. Notably, the indolium segment of the probe exhibited the lowest rotational energy, quantified at 7.38 kcals/mol. The probe featured heightened mitochondrial viscosity dynamics when contained within HeLa cells subjected to agents like nystatin, monensin, and bacterial lipopolysaccharide (LPS). Overall, our innovative methodology elucidates intricate mitochondrial factors, presenting transformative insights into cellular energetics, redox homeostasis, and therapeutic avenues for mitochondrial-related disorders.

1. Introduction

Mitochondria, the multifunctional organelles best known for their role in ATP production through oxidative phosphorylation, are central players in eukaryotic cell biology. [1–17] Beyond energy generation, these dynamic double-membraned structures actively orchestrate a spectrum of cellular processes, including apoptosis, calcium signaling, biosynthesis, and quality control mechanisms to maintain their health. [3–19] The integrity of mitochondrial function is pivotal for overall cellular health and functionality. Recent evidence suggests that two emerging factors within mitochondria, viscosity and sulfur dioxide (SO_2) levels, provide crucial insights into organelle functionality. [20–32] Viscosity, a term denoting the thickness and fluidity of the intracellular milieu, is a pivotal parameter that profoundly influences mitochondrial dynamics. [3–17,33–36] It impacts molecular diffusion, membrane dynamics, and biochemical reactions within mitochondria. [33–36] Appropriate mitochondrial matrix viscosity is essential for the movement of proteins, metabolites, and ions crucial for oxidative phosphorylation and other vital mitochondrial processes. [3–17,33–36] Dysregulated viscosity has been implicated in neurodegenerative

* Corresponding author at: Department of Chemistry, Michigan Technological University, Houghton, MI 49931, United States of America.
E-mail addresses: sdwive2@mtu.edu (S.K. Dwivedi), rluck@mtu.edu (R.L. Luck), hyliu@mtu.edu (H. Liu).

https://doi.org/10.1016/j.jphotobiol.2024.112986
Received 23 March 2024; Received in revised form 28 June 2024; Accepted 9 July 2024
Available online 11 July 2024

disorders, diabetes, and cancer, emphasizing its role in elucidating mechanisms of mitochondrial dysfunction. [3–17,33–36]

Alternatively, SO_2 can originate from sulfur-containing amino acids and the oxidation of hydrogen sulfide in vivo, eventually forming sulfite (SO_3^{2-}) and bisulfite (HSO_3^-) derivatives within cells [37]. Endogenous SO_2, a metabolite of hydrogen sulfide and sulfur-containing amino acids, plays roles in various physiological processes crucial for body equilibrium. Deviations in these molecules' levels can result in neurological, respiratory, cardiac, and pulmonary diseases. However, the exact pathogenic roles of endogenous SO_2 remain incompletely understood [38]. SO_2 is a prevalent air pollutant, emitted mainly from volcanic eruptions and industrial activities, persisting for decades. Additionally, it serves as a venom. Furthermore, SO_2 and its derivatives are commonly utilized as food antiseptics due to their antibacterial, bleaching, and antioxidant properties. Nonetheless, excessive consumption of these additives can trigger allergic reactions and irreversible tissue damage in some individuals. To address this, the World Health Organization (WHO) and Food and Agriculture Organization (FAO) strictly regulate the levels of SO_2 and its derivatives in food. Thus, monitoring their concentrations both in vivo and in vitro is imperative [20–32,39]. As the primary intracellular source of sulfur-containing and reactive oxygen species, real-time monitoring of mitochondrial SO_2 dynamics could provide pivotal insights connecting concentration-dependent effects to regulation of energetics, redox homeostasis and mitochondrial dysfunction. Clarifying SO_2's emerging regulatory roles specifically within mitochondria has the potential to uncover novel therapeutic targets and interventions for mitochondrial disorders. [20–32,39] Similarly, cellular viscosity plays a pivotal role at the cellular level. Anomalous intracellular viscosity can disrupt the activity of membrane-binding proteins and hinder insulin synthesis, leading to related diseases. For instance, mitochondrial matrix viscosity is closely associated with the onset of various diseases, including neural degenerative diseases, Parkinson's disease, Alzheimer's disease, and atherosclerosis [40]. Changes in viscosity can elucidate interactions between biomolecules and the transport of metabolic waste by altering biomolecule mobility within cells, thus causing intracellular disturbances. These disturbances impact the diffusion of short-lived active intermediates, such as reactive oxygen species during oxidative stress. Unfortunately, established viscosity measurement devices like capillary viscometers, rotational viscometers, and drop ball viscometers are inadequate for measuring viscosity changes at the cellular level.

In this study, we have developed a dual-channel fluorescent probe that enables the simultaneous monitoring of mitochondrial viscosity and SO_2 levels in living cells. To create this advanced probe, electron-withdrawing acceptors (1,3,3-trimethyl-3H-indolium and 1-methylquinolinium) were incorporated into a coumarin dye at 2,3-positions, respectively. (Scheme 1). This innovative probe introduces a unique capability for conducting ratiometric fluorescence quantification and imaging of sulfur dioxide (SO_2). It features distinct fluorescence peaks at 650 nm and 558 nm, producing a 92 nm blue-shifted fluorescence spectrum activated by SO_2, free from interference by NAD(*P*)H and other reactive sulfur species like cysteine, homocysteine, glutathione, and H_2S. When excited at 500 nm, the probe demonstrates a decrease in fluorescence at 650 nm and an increase at 558 nm. Furthermore, this probe enables near-infrared fluorescence determination of viscosity, exhibiting fluorescence enhancement at 658 nm under 570 nm excitation in glycerol. Probe **A** has demonstrated versatile capabilities in monitoring intracellular viscosity dynamics induced by various stimulants in HeLa cells. We subjected HeLa cells with chemical agents known to disrupt membrane integrity and ion homeostasis including the antifungal nystatin, the ionophore monensin, and a key immune activator in bacterial lipopolysaccharide (LPS). Pretreatment with each of these distinct stimuli elicited a significant elevation in mitochondrial viscosity reported by our probe compared to control cells. Our dual-probe approach, shedding light on mitochondrial viscosity and SO_2 dynamics in situ, holds the potential to uncover mechanisms associated with mitochondrial dysfunction. The methodology establishes a new platform for visualizing and elucidating the intricate interplay among these crucial factors. This includes their contributions to cellular energetics, redox homeostasis, and disease states, presenting new avenues for further exploration in disorders related to mitochondria.

2. Results and Discussion

2.1. The Probe Synthesis

Coumarin dyes combine several advantageous properties: they exhibit high molar absorptivity for efficient light capture, boast excellent fluorescence quantum yields for bright photon emission, feature large Stokes shifts that prevent self-quenching by separating excitation and emission, offer tunable emission wavelengths through substituent modifications, and respond dynamically to environmental changes, reflecting biochemical conditions. [41–47] Moreover, many derivatives of coumarin showcase notable photostability. [41–43] To enable the

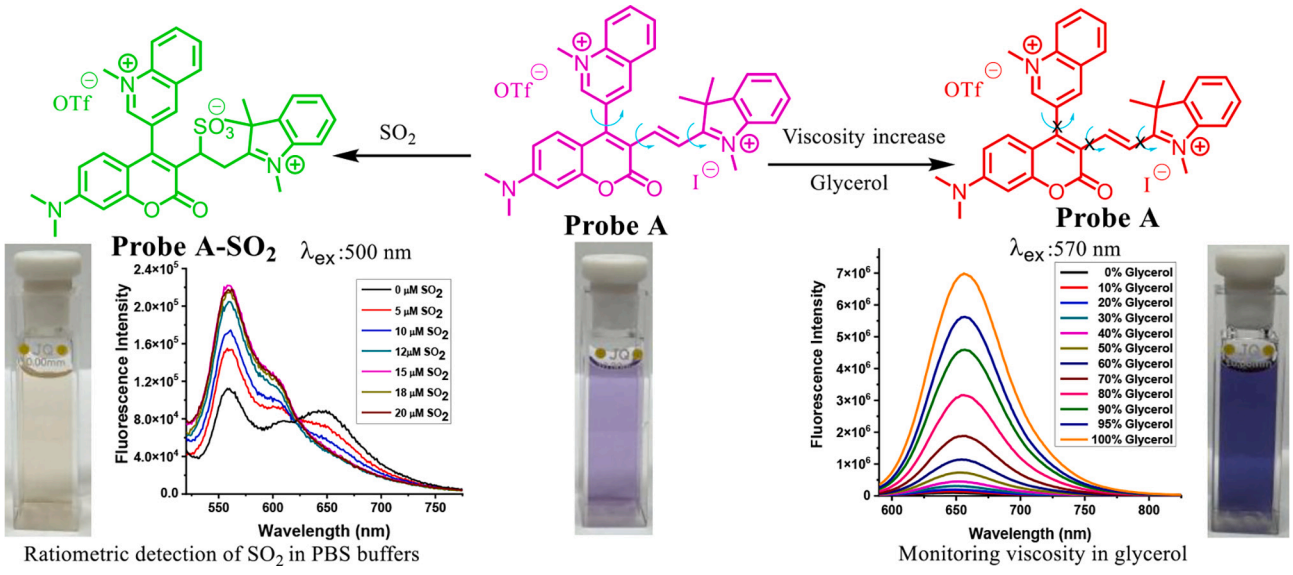

Scheme 1. Probe's sensing of viscosity and SO_2.

detection of viscosity and achieve ratiometric SO_2 detection using dual fluorescence channels in live cells, we utilized a coumarin platform by integrating a 3-quinolinium acceptor moiety into the 3-position of the coumarin hemicyanine dye for probe **A** (Scheme 2). To execute this approach, we synthesized 4-chloro-2-oxo-2H-chromene-3-carbaldehyde (**3**) following established procedures, Scheme 2. Subsequently, a palladium-catalyzed Suzuki reaction between the coumarin derivative (**3**) and (quinolin-3-yl)boronic acid (**4**) yielded 7-(dimethylamino)-2-oxo-4-(quinolin-3-yl)-2H-chromene-3-carbaldehyde (**5**). Probe **A** was synthesized via a condensation reaction between compound **5** and 1,2,3,3-tetramethyl-3H-indol-1-ium iodide (**6**), yielding (E)-2-(2-(7-(dimethylamino)-2-oxo-4-(quinolin-3-yl)-2H-chromen-3-yl)vinyl)-1,3,3-trimethyl-3H-indol-1-ium iodide (**7**), followed by the methylation of compound **7**. The intermediates and probe **A** were characterized using both NMR and mass spectrometry techniques.

2.2. Optical Study of Probe A

Initially, we assessed the compatibility of probe **A** across solvents of varying polarities. We monitored the absorption and emission spectra of probe **A** (10 μM) in solvent systems including ethanol, DMSO, 1,4-dioxane, chloroform, ethyl acetate, acetonitrile, water, and toluene. Notably, probe **A** exhibited minimal modulation in absorption and emission spectra at their respective excitation wavelengths except from 1,4-dioxane (Fig. S8, Table S1). Probe **A** exhibited strong emission in 1,4-dioxane compared to other solvents. Conversely, in an aqueous environment, it showed a reduction in emission intensity at 658 nm. The changes in emission intensity relative to the water fraction in the nonpolar dioxane solvent are depicted in Fig. S9. It was observed that as the water fraction increased, the fluorescence intensity gradually decreased. This finding suggests that probe **A** can be used in live cells without being affected by the aqueous environment of the cellular compartment.

We explored the impact of viscosity on the optical properties of probe **A** within pH 7.4 PBS buffers containing varying glycerol concentrations. By modulating the glycerol-to-PBS buffer volume ratio, the absorbance of probe **A** displayed shifts in absorption peaks slightly, notably around 589 nm, ranging from 0% to 100% glycerol content in the solutions (Fig. 1, left). Intriguingly, under an excitation wavelength of 570 nm, the fluorescence intensity of probe **A** at 658 nm surged by a remarkable 81-fold (Fig. 1, right). A linear relationship exists between log(I_{max}) and log (viscosity) with a correlation coefficient of 0.98 (Fig. S10), indicating that the probe **A** is apposite for quantitative determination of the viscosity. Additionally, when we excited probe **A** at 500 nm, we detected a weak fluorescence at 568 nm alongside a robust emission at 658 nm. Conversely, upon excitation at 400 nm, two distinct strong emission wavelengths emerged at 658 nm and 460 nm (Fig. S11). This enhancement can be attributed to the elevated viscosity in the probe solution. As viscosity increased, it constrained the free rotation of individual sp^2-hybrid carbon-carbon bonds within probe **A** (Scheme 1). This restricted rotation effectively curtailed the dissipation of excited photon energy due to molecular movement. Consequently, as solution viscosity intensified, there was a pronounced amplification in the fluorescence intensity of the probe (Fig. 1).

In our investigation of the optical properties of probe **A**, we delved into the influence of varying concentrations of HSO_3^- using UV–visible and fluorescence titration methods. Upon introducing HSO_3^- concentrations ranging from 0 to 15 μM into a pH 7.4 PBS buffer with 10 μM of probe **A**, showed linear response upto 15 μM (Fig. S12) and notable shifts in absorption characteristics were observed. Specifically, the probe's absorption peak at 580 nm diminished progressively as the HSO_3^- concentration increased (Fig. 2, left). Concurrently, a distinct absorption peak emerged at 410 nm, intensifying with rising HSO_3^- levels (Fig. 2, left). This alteration suggests a disruption in the probe's π-conjugation when exposed to HSO_3^-. Furthermore, probe **A** showcased ratiometric fluorescence behaviors in response to HSO_3^- (Fig. 2, right). As the HSO_3^- concentrations escalated, fluorescence intensity reduced at 650 nm while concurrently increasing at 558 nm (Fig. 2). This fluorescence modulation is attributed to the bisulfite-induced disruption of the probe's π-conjugation, a consequence of the probe's interaction with bisulfite. To corroborate this interaction, mass spectrometry analysis was employed, confirming our hypothesis of the probe π-conjugation disruption by disulfide through an addition reaction (Scheme 1 and Fig. S7). Moreover, we subjected probe **A** to excitation at both 400 nm and 570 nm. Upon excitation at 400 nm, we observed a faint fluorescent band at 510 nm, which exhibited a slight increase in fluorescence emission upon the addition of HSO_3^-. Conversely, upon excitation at 570 nm, a prominent fluorescent band emerged at 650 nm, demonstrating a decrease in fluorescence intensity following the addition of HSO_3^- (20 μM) (Fig. S13).The comprehensive nature of these observations underscores the intricate and dynamic optical responses of probe **A** in the presence of different concentrations of HSO_3^-. Furthermore, we investigated the impact of HSO_3^- on probe **A** in the presence of viscosity, specifically in a 90% glycerol solution. We observed a decrease in the band at 658 nm, accompanied by the formation of a new band at 568 nm with reduced fluorescence intensity upon excitation at 500 nm. Similarly, following excitation at 570 nm, the band at 658 nm diminished upon addition of HSO_3^- (15 μM) (Fig. S14).

2.3. Theoretical Calculations

Procedures used to conduct these calculations are given in the supporting information and they follow methods detailed previously. [48] Probe **A** consists of three distinct segments, 7-(dimethylamino)-2*H*-chromen-2-one linked to 1,3,3-trimethyl-3*H*-indol-1-ium via an ethylene bridge constituting a planar section and a 1-methylquinolin-1-

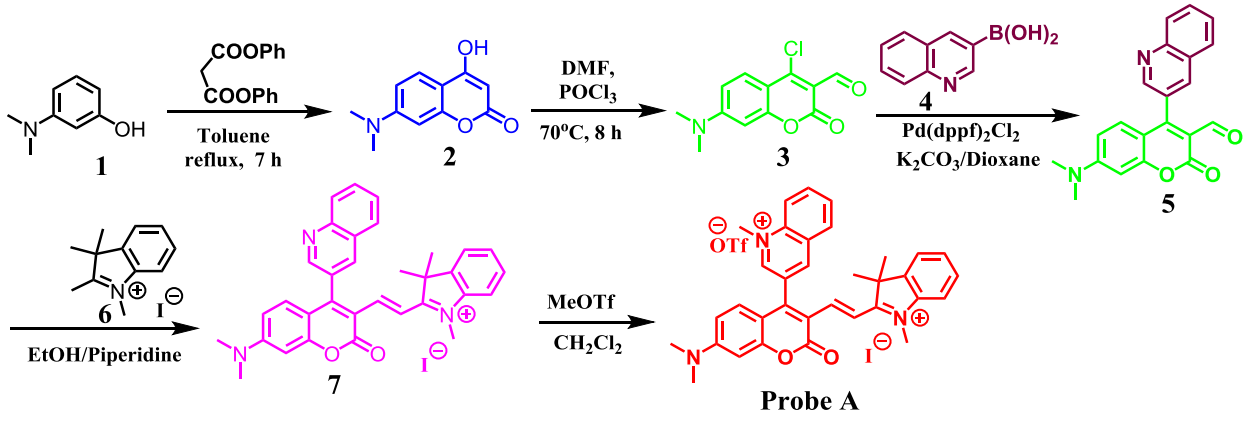

Scheme 2. Synthetic method to prepare probe **A** for sensing viscosity and SO_2.

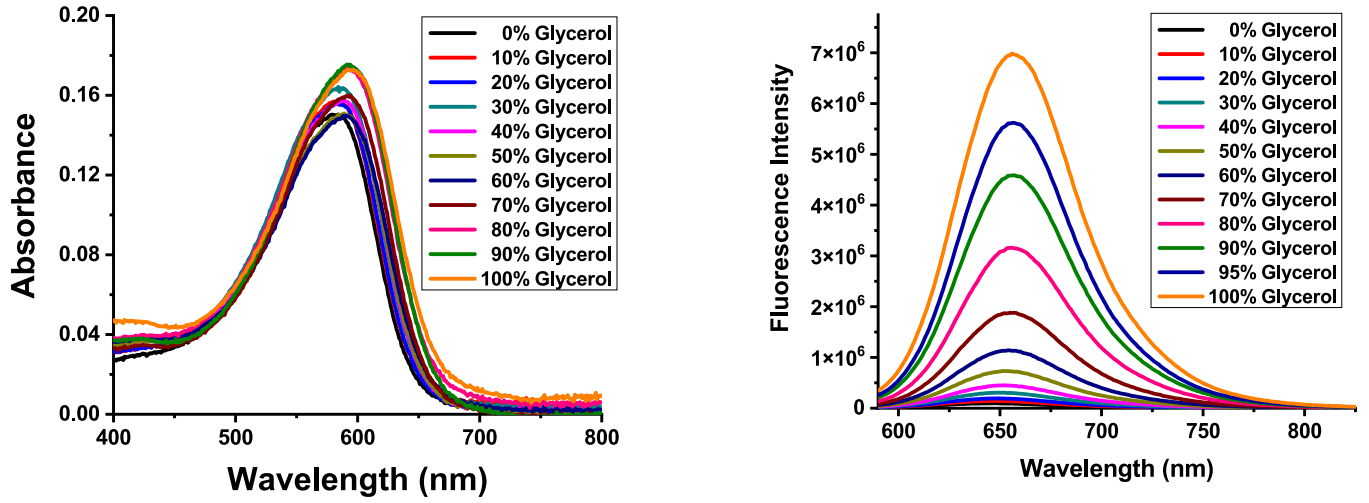

Fig. 1. Absorption spectra (left) and fluorescence spectra (right) of probe **A** (10 μM) in mixed solutions with various ratios of pH 7.4 PBS buffer to glycerol, recorded under excitation at 570 nm.

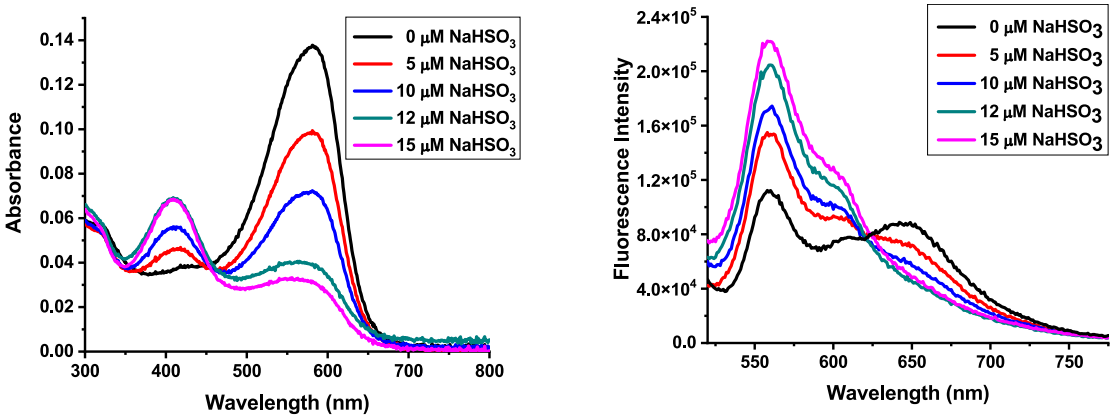

Fig. 2. Absorbance spectra (left) and fluorescence spectra (right) of 10 μM probe **A** in the absence and presence of different concentrations of $NaHSO_3$ in pH 7.4 PBS buffers under excitation at 500 nm.

ium moiety situated at 59.80° to this plane arranged as shown in Fig. 3.

As depicted in Scheme 1, probe **A** reacts with SO_2 and this results in the two isomers, *R* and *S*, shown in Fig. 3. As is evident in the current density illustration in Fig. 4, the coordination of SO_2 disrupts the planar arrangement of the chromenone and indolium moieties and orients the plane of the quinolinum group at 87° to the chromenone in both isomers. Interestingly in all cases, there is no evidence of orbital involvement in the absorption of probe **A** by the quinolinum moiety, judging by the lack of current density evident in Fig. 4. In probe **A**, the transition originates from the N atom on the left side of the chromenone and goes over to the right side where the electron-withdrawing O atoms are situated with some extension into the indolium moiety. The SO_2 coordination disrupts the planar arrangement and in the case of both isomeric forms, the transition is localized on the chromenone moiety.

Probe **A** also displays a consistent absorption irrespective of changes in viscosity produced by using mixed solutions with various ratios of pH 7.4 PBS buffer to glycerol, Fig. 1. In contrast, increases in fluorescence under excitation at 570 nm were observed as the solutions became more viscous. Unfortunately, the limited solubility of probe **A** in solvents that can attain low temperatures prevented resolution of this by variable temperature NMR. There are three locations where the molecule can rotate and dissipate absorption energy via non-radiative mechanisms. These calculations were conducted in a glycerol medium and are illustrated in Figs. S24-S26. The rotation of the indolium moiety contained two different activation energy barriers at 7.38 and 8.88 kcals/mol relating to the two perpendicular orientations with the higher energy occurring when the dimethyl substituents on the indolium moiety were closest to the methyl substituent on the quinolinum group, Fig. S24. The rotation of the ethylene bridge plus indolium also contained two activation energy levels at 11.03 and 12.03 kcals/mol and these also occur

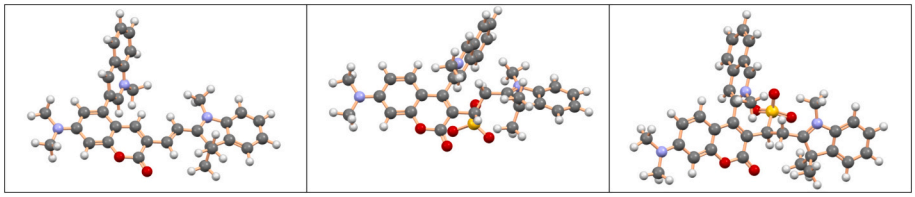

Fig. 3. Mercury [49] drawings of probes **A** (left), **(*R*)-A-SO_2** (middle), and **(*S*)-A-SO_2** (right).

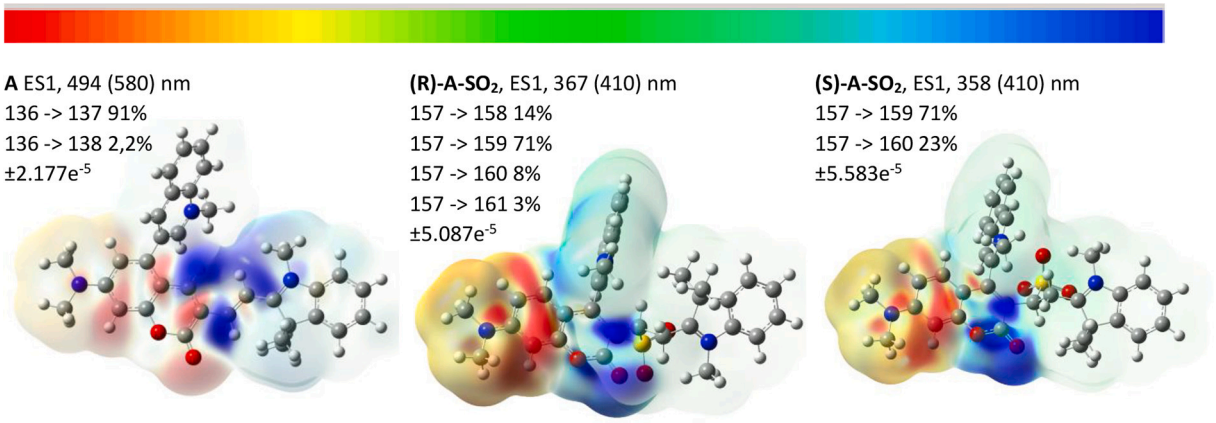

Fig. 4. The schematic representation of variances in current density is depicted as isosurfaces corresponding to the probes **A**, **(*R*)-A-SO$_2$**, and **(*S*)-A-SO$_2$**. The quantity of energized states (ES), both the theoretically derived and experimentally observed wavelengths, alongside the transitions, are detailed in conjunction with their proportional contribution percentages. The values that correspond to the color grading atop the figure are also enumerated. For further elucidation, diagrams related to the numerically labeled LCMOs are included in the supplementary data provided.

when this fragment is perpendicular to the chromenone, Fig. S25. The rotation of the quinolinum group required the highest activation barrier at 12.32 and 11.00 kcals/mol with the higher activation barrier occurring when the methyl group on the quinolinum group was closest to that on the indolium, Fig. S26. These differences in rotational energies are not large and even though the calculations were conducted in glycerol (consisting of the addition of a dielectric constant to the calculation), no differences in energies of rotation were noted in glycerol and water as the solvents. It is possible to include additional explicit molecules of solvation which may illustrate these differences, but it would be difficult to know exactly how the molecule or molecules of solvation would be arranged. Interestingly, positioning one glycerol molecule in an interactive state with probe **A,** as shown in Fig. 5. This contained a H-bond between a H atom on glycerol and an O atom on probe **A** at a distance of 1.930 Å and a dipole interaction between a lone pair on an O atom on glycerol and the positively charged N atom on probe **A** at 3.011 Å, full details in Supporting Information. This interaction would not allow for rotation in this indolium section of the molecule, but we note that the effect is not stoichiometric as there is a huge increase in the concentration of glycerol compared to the probe required to register an effect in the viscosity studies. Therefore, it is likely that such localized interactions may require a more extended arrangement of glycerol molecules to reduce rotations. There is a slight reduction in the calculated absorption with this glycerol adduct at 460 nm, Fig. 5, compared to that calculated for pure probe **A** at 494 nm.

2.4. The Probe Selectivity to Viscosity

Mitochondria contain diverse active small molecules that could potentially interfere with fluorescent probes. To verify the selectivity of probe **A** for viscosity, we evaluated common metal ions, inorganic ions, and amino acids. Probe **A** exhibited negligible spectral interference upon exposure to potentially disruptive species including Co^{2+}, Fe^{3+}, Ca^{2+}, K^{+}, Na^{+}, Cl^{-}, SO_4^{2-}, CN^{-}, NO_2^{-}, glycine, lysine, methionine, glutathione, and cysteine (Fig. 6) at 570 nm excitation. Conversely, altering solution viscosity induced significant fluorescence changes, even in the presence of these species. Likewise, we conducted selectivity experiments with probe **A** using SO_2 under 500 nm excitation. Probe **A** demonstrated minimal spectral interference when exposed to various ions and amino acids (Fig. 6).

Cuvette experiments were conducted by adding monensin to probe **A** in a PBS buffer solution, and no significant change in fluorescence emission was observed (Fig. S30). These results indicate that the increase in intracellular fluorescence is attributed to the increase in viscosity within the mitochondria. Therefore, probe **A** could be used as a mitochondrial viscosity probe to monitor metabolic changes in mitochondria (Fig. S30).

2.5. Photostability and pH Effect on the Fluorescent Probe

We also evaluated the photostability of probe **A** by examining its emission spectra (Fig. S31). Under excitation at 570 nm in 100% glycerol, we observed that probe **A** maintained its fluorescence intensity

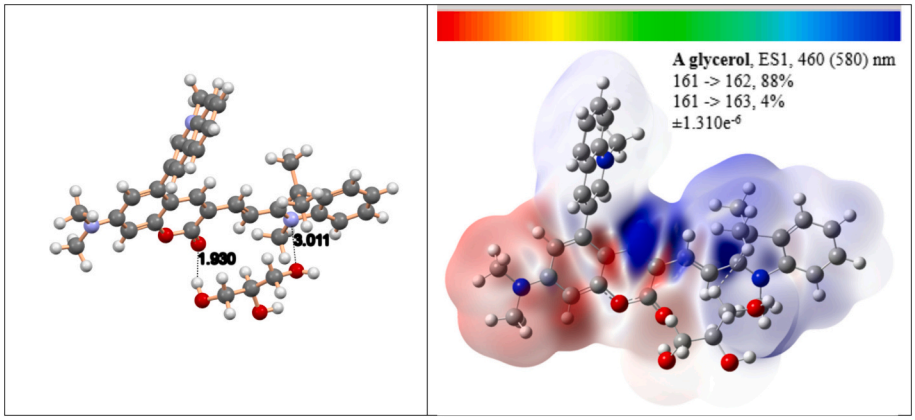

Fig. 5. Mercury [49] drawing of the location of one molecule of glycerol with probe **A** with distances indicated in Å (left) and current density illustration (right).

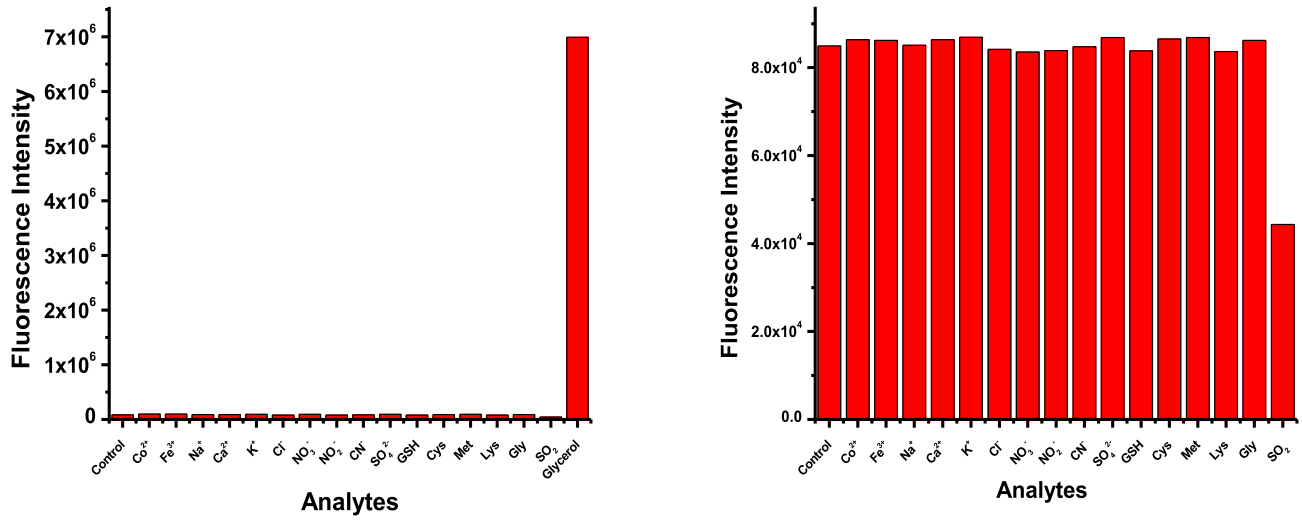

Fig. 6. Selectivity of probe **A** towards viscosity (left) and SO_2 (right) over common interfering species. Fluorescence intensity of probe **A** (10 μM) at 650 nm with excitation at 570 nm and 500 nm, respectively in pH 7.4 PBS buffer. Various concentrations of potentially interfering species (100 μM Co^{2+}, Fe^{3+}, Na^{+}, Ca^{2+}, K^{+}, Cl^{-}, NO_3^-, NO_2^-, CN^-, SO_4^{2-}, 100 μM glycine (Gly), lysine (Lys), methionine (Met), glutathione (GSH), cysteine (Cys); 15 μM bisulfite (HSO_3^-)) and 100% glycerol (viscosity control) were evaluated.

remarkably well over a period of 2 h, with no significant loss in relative fluorescence intensity. Further, to comprehensively assess the suitability of a fluorescent probe for studying viscosity within live cells, it is crucial to understand its behavior in relation to pH variations. This ensures that the observed fluorescence changes are solely attributable to viscosity alterations and not confounded by pH-induced effects (Fig. S32). In our study, we rigorously evaluated the pH sensitivity of the fluorescence probe. Specifically, we recorded fluorescence spectra of a 10 μM concentration of probe **A** across various pH conditions using distinct PBS buffers, with excitation set at 500 nm. In an acidic medium (pH 3.6) (Fig. S32A), probe **A** showed insignificant changes in the emission spectrum after interaction with HSO_3^-. However, at pH 7.4, probe **A** exhibited ratiometric fluorescence behavior in response to HSO_3^- (Fig. 2, right, and Fig. S32B). As HSO_3^- concentrations increased, fluorescence intensity decreased at 650 nm while increasing at 558 nm (Fig. 2 and Fig. S32B). Conversely, in basic media (pH 7.8 and 8.6), there was an enhancement in the emission spectrum (Fig. S32C and S32D). Encouragingly, our findings conclusively demonstrate that probe **A** exhibits minimal sensitivity to pH fluctuations. This lack of pH dependence is pivotal for accurate viscosity measurements within live cells. By ensuring that the fluorescence intensity of the probe remains consistent across different pH environments, we can confidently attribute any observed changes in fluorescence to alterations in cellular viscosity alone. Consequently, this enhances the reliability and interpretability of our viscosity data, allowing for more precise insights into cellular dynamics and function.

2.6. Cell Viability Assessment of Probe A on HeLa Cells Using MTT Assay

To evaluate the cytotoxicity of probe **A** on HeLa cells, an MTT (3-(4,5-dimethylthiazol-2-yl)-2,5-diphenyltetrazolium bromide) assay was conducted. The MTT assay is a widely accepted method for assessing cell viability based on the metabolic activity of cells. [50–53] The MTT assay results affirm the biocompatibility of probe **A** with HeLa cells, revealing >90% cell viability at a concentration of 50 μM over 48 h (Fig. S33). These findings lay a solid foundation for further exploration and potential applications of probe **A** in live-cell imaging, monitoring, and related cellular studies.

2.7. Assessing Changes in Cellular Viscosity

The assessment of intracellular viscosity serves as a critical tool to elucidate fundamental cell biology and pathology. Viscosity strongly governs molecular diffusion rates inside cells, dictating biochemical reaction kinetics and signaling pathway activation. Abnormal viscosity also hinders organelle movements along cytoskeletal tracks, disrupting intracellular trafficking and dynamics. Beyond basic cell biology, deviations in intracellular viscosity have been associated with specific diseased states like cancer, diabetes, and neurodegeneration. [3–17,33–36] Cancer cells often display heightened viscosity compared to normal cells, which may promote metastasis by enhancing cell migration and compromising immune surveillance. [54] Elevated viscosity in diabetes impairs insulin signaling and glucose uptake. [55] In Alzheimer's disease, increased tau protein viscosity in neurons correlates with neurotoxic aggregate formation. [56,57] Thus, quantitative viscosity measurements in live cells could shed light on disease mechanisms and serve as a biomarker for diagnosis and treatment monitoring. Simple intracellular viscosity probes like molecular rotors provide an accessible way to investigate these dynamics in various cell types. Going forward, improved viscosity detection techniques and probes will enable more accurate measurements in complex tissue microenvironments. [57] Overall, evaluating intracellular viscosity facilitates the examination of fundamental cellular processes and the investigation of links between abnormal viscosity and human disease. [57]

We hypothesize that the dual positive charges carried by probe **A** can significantly augment its affinity and precision in targeting mitochondria. These positive charges are likely to facilitate interactions with negatively charged constituents or specific receptors within the mitochondrial environment, thereby ensuring precise and efficient localization. To validate this conjecture, we conducted a co-localization experiment by exposing HeLa cells to 5 μM Nystatin for 30 min, followed by simultaneous incubation of probe **A** with the mitochondria-targeting agent, Mito View 405 (Fig. 7). The notable correlation coefficient of 0.955 observed between our probe, probe **A**, and the mitochondria-specific Mito View 405 underscores the reliability and robustness of our probe's targeting mechanism (Fig. 7). This elevated correlation coefficient signifies an almost flawless association between the two probe markers, highlighting the exquisite precision with which probe **A** targets in on mitochondria. Additionally, we employed ER Tracker and Lyso-Tracker dyes at a concentration of 5 μM to verify the localization of probe **A** within mitochondria rather than within the endoplasmic reticulum and lysosomes. The obtained correlation coefficients were 0.759 and 0.776, respectively (Fig. S34 and S35).

In our initial investigation, we leveraged the capabilities of probe **A**

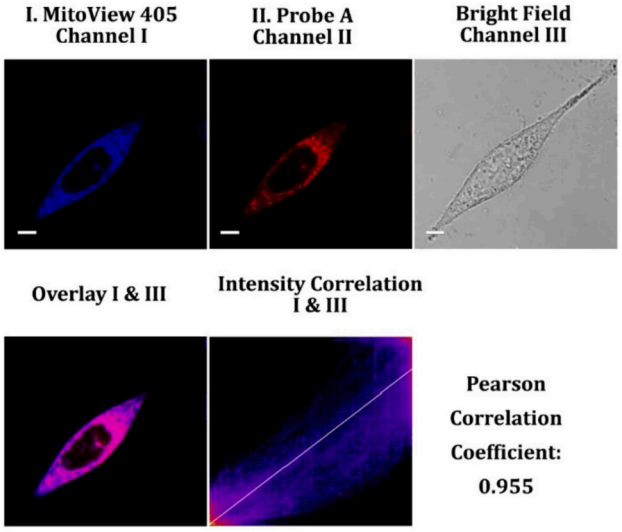

Fig. 7. Fluorescence microscopy images illustrating HeLa cells following treatment with 5 μM Nystatin for 30 min, followed by incubation with 5 μM MitoView 405 and 5 μM probe **A** for 20 min. The blue fluorescence signal emitted by MitoView 405, captured between 425 nm and 475 nm upon excitation at 405 nm, highlights mitochondrial localization. Meanwhile, the red fluorescence corresponding to probe **A**, acquired from 630 nm to 730 nm using 559 nm excitation, indicates intracellular distribution. Scale bar = 20 μm. (For interpretation of the references to color in this figure legend, the reader is referred to the web version of this article.)

to probe viscosity changes within HeLa cells. To induce modifications in cellular characteristics and assess their effect on viscosity, we treated the cells with the antifungal agent Nystatin. By disrupting the cell membrane's ergosterol and permeability, Nystatin has been reported to indirectly lead to increased intracellular viscosity and molecular crowding. [57] After administering Nystatin for 20 min, we further incubated HeLa cells with probe **A** to directly measure changes in viscosity within this cellular environment. To validate our findings and establish a comparative basis, we also executed control experiments. In these controls, HeLa cells were solely exposed to probe **A** without any Nystatin treatment, aiming to understand the inherent fluorescence properties without external viscosity-altering agents. Upon thorough analysis, a notable fluorescence pattern emerged: cells treated with Nystatin exhibited a significant increase in fluorescence compared to untreated cells. This enhanced fluorescence effectively indicates heightened intracellular viscosity following Nystatin exposure (Fig. 8).

Monensin, primarily utilized as a coccidiostat, serves to prevent and manage coccidiosis, a parasitic ailment induced by coccidian protozoa, commonly affecting various animals including poultry and livestock. Its mechanism involves disturbing the development of these protozoa within the animal's intestinal tract, thereby managing the infection. [58–60] Apart from its veterinary application, Monensin has been employed as a growth enhancer in cattle feed to enhance feed efficiency and stimulate weight gain. [61] However, its use for this purpose faces restrictions or bans in numerous countries due to concerns regarding antibiotic resistance development and potential adverse effects on animal health and food safety. To assess the impact of Monensin treatment on intracellular viscosity, HeLa cells were subjected to incubation with fluorescence viscosity probe **A**, targeting mitochondria, either with or without prior Monensin treatment. Monensin-treated cells exhibited heightened fluorescence compared to control cells (Fig. 9), indicating a substantial increase in mitochondrial viscosity induced by this ionophore. Monensin, known for its multifaceted impact on cellular physiology, intriguingly increases cell viscosity. This phenomenon stems from its ability to perturb various cellular processes. By modulating ion concentrations across membranes, particularly calcium levels crucial for cytoskeletal organization, Monensin induces cytoskeletal rearrangements that alter cell morphology and viscosity. [62,63] Additionally, it disrupts membrane fluidity and protein glycosylation, affecting cell surface properties and interactions. Disruption of osmotic balance further contributes to changes in cell volume and internal pressure, indirectly influencing viscosity. The collective effect of these alterations underscores the intricate interplay between Monensin and cellular dynamics, shedding light on its diverse physiological consequences. [62]

Bacterial lipopolysaccharide (LPS), located primarily in the outer membrane of Gram-negative bacteria, is a complex molecule comprised of lipid A, core oligosaccharide, and O antigen. [64] By eliciting a robust immune response, LPS plays a pivotal role in the pathogenesis of Gram-negative bacterial infections. [64] Specifically, LPS triggers the release of pro-inflammatory cytokines such as interleukin-1 (IL-1), tumor necrosis factor-alpha (TNF-α), and interleukin-6 (IL-6) from immune cells.

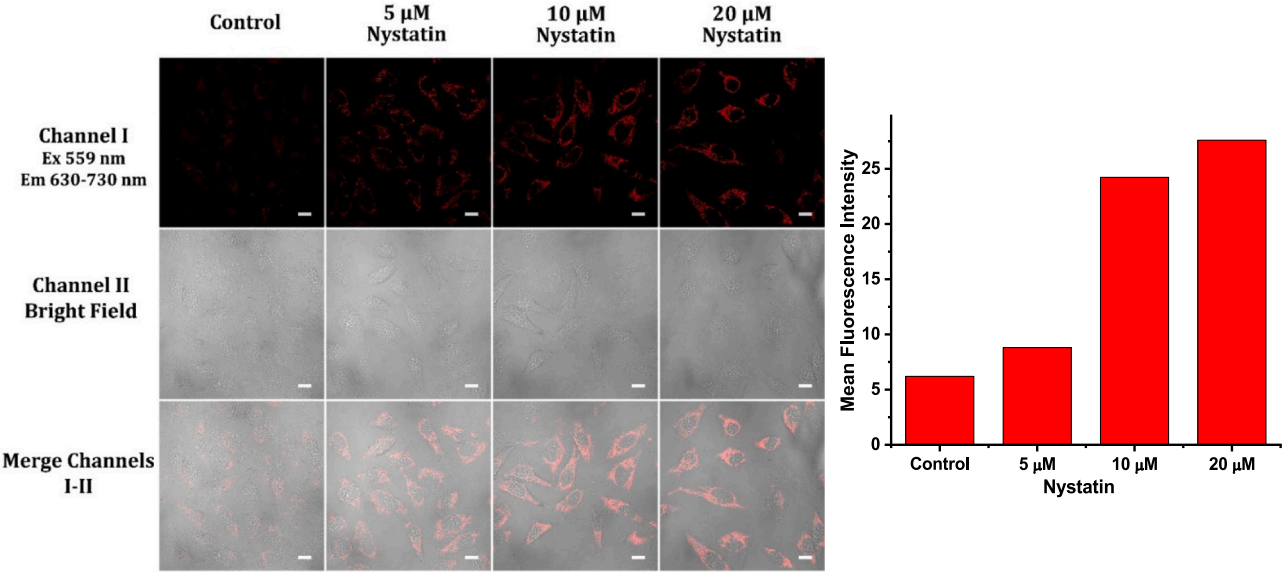

Fig. 8. Confocal laser fluorescence microscopy images depicting HeLa cells treated with varying concentrations of Nystatin (0 μM as control, 5 μM, 10 μM, and 20 μM) for 30 min, followed by subsequent incubation with probe **A** (5 μM) for an additional 20 min. Imaging was conducted between 630 nm and 730 nm using a 559 nm excitation wavelength. Scale bar = 50 μm. Histograms depicting the fluorescence intensity of probe **A** (5 μM) at various concentrations of Nystatin (right).

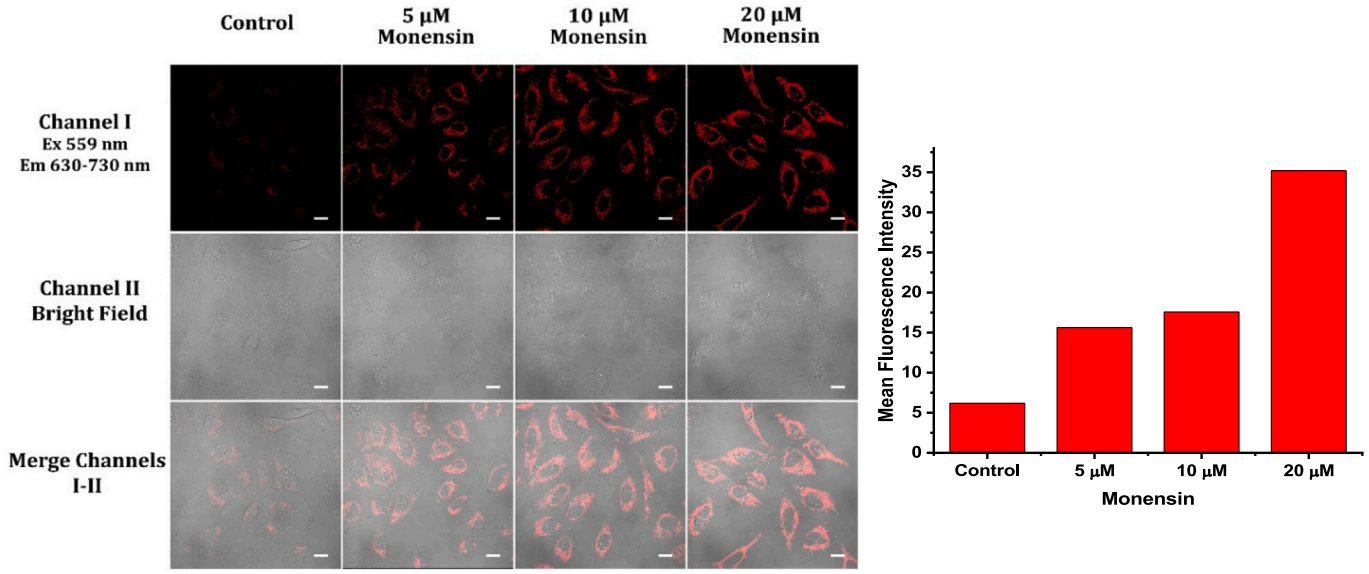

Fig. 9. Fluorescence microscopy images depicting HeLa cells treated with varying concentrations of Monensin (0 μM as control, 5 μM, 10 μM, and 20 μM) for 30 min, followed by incubation with probe **A** (5 μM) for an additional 20 min. Fluorescence was captured within the 630 nm to 730 nm wavelength range, utilizing a 559 nm excitation source. Scale bars represent 50 μm. Histograms displaying the fluorescence intensity of probe **A** (5 μM) at varying concentrations of Monensin (right).

[65,66] This cytokine release induces fever, inflammation, and other systemic effects known collectively as endotoxemia. [65,66] In severe cases, the excessive immune response can lead to potentially life-threatening septic shock and multiple organ failure. [65,66] Beyond its role in infection, LPS is a crucial model for studying immune response and inflammation with applications in vaccine development, drug discovery, and understanding infectious disease. In our study, we utilized probe **A** to explore LPS's impact on cellular viscosity in HeLa cells, revealing a significant increase in viscosity upon LPS treatment, evidenced by heightened fluorescence compared to controls, Fig. 10. This rise in viscosity stems from LPS-induced mitochondrial reactive oxygen species (ROS) production, which enhances electron transport chain activity, leading to oxidative damage and matrix expansion through protein unfolding. The resulting cellular swelling induces molecular crowding, further elevating intracellular viscosity. Additionally, LPS stimulation induces dynamic alterations in mitochondrial ultrastructure, triggering both fission and fusion events that remodel the inner mitochondrial membrane, potentially introducing diffusion bottlenecks and hindering molecular transport within the organelle.

Mitophagy, a crucial cellular process, selectively degrades mitochondria, the energy-generating organelles. [67] During starvation, cells adapt to conserve energy, inducing autophagy, where cellular components are degraded and recycled for energy and building blocks. Mitophagy is vital in this context, maintaining cellular balance by eliminating dysfunctional mitochondria and recycling components for energy production, optimizing function, and preventing toxic byproducts. [68] Molecular mechanisms, like the AMPK and mTOR pathways, regulate mitophagy during starvation, promoting cell survival. [68] We

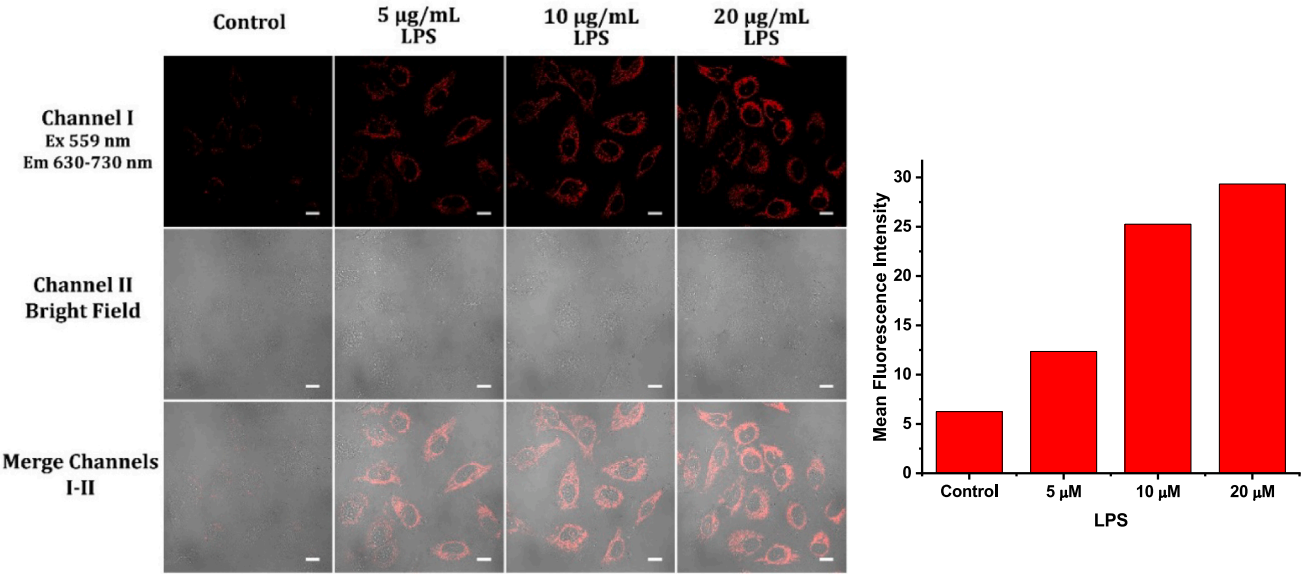

Fig. 10. Fluorescence microscopy images illustrating HeLa cells exposed to varying concentrations of LPS (0 μg/mL as control, 5 μg/mL, 10 μg/mL, and 20 μg/mL) for 30 min. Subsequent incubation with probe **A** (5 μM) was conducted for an additional 20 min. Fluorescent emissions were recorded between 630 nm and 730 nm using a 559 nm excitation wavelength. Scale bars denote 50 μm. Histograms illustrating the fluorescence intensity of probe **A** (5 μM) at different concentrations of LPS (right).

used a mitochondria-targeting probe **A** to examine mitochondrial viscosity in HeLa cells during mitophagy induced by starvation. [69–71] Cells treated with probe **A** in serum-free media showed increasing fluorescence over time, suggesting mitochondrial adaptations to nutrient deprivation, Fig. 11. Starvation triggers mitochondrial quality control pathways, such as mitophagy, removing damaged mitochondria, and inducing metabolic and compositional changes to promote survival. These adaptations likely affect mitochondrial matrix viscosity, influenced by factors like protein composition and molecular crowding. Increasing probe **A** fluorescence indicates gradual changes in mitochondrial microenvironment and viscosity during starvation. Plausible explanations include protein or lipid accumulation, cristae structure remodeling, matrix condensation, or metabolic enzyme and pathway modifications. We propose that changes in mitochondrial viscosity during starvation aid in metabolic regulation, quality control, or signaling mechanisms, ensuring cell viability.

To evaluate sulfur dioxide levels within HeLa cells, we utilized probe **A**, initially treating the cells with varying $NaHSO_3$ concentrations (0 μM as control, 5 μM, and 10 μM) for 30 min. Following this treatment, a subsequent 20-min incubation with probe **A** (5 μM) unveiled distinctive fluorescence responses in bisulfite-exposed cells (Fig. 12). Notably, these cells manifested ratiometric fluorescence changes suggestive of sulfur dioxide presence. Specifically, the green channel exhibited a progressive enhancement in fluorescence intensity, while the red channel concurrently displayed a diminishing fluorescence intensity. Such fluorescence dynamics resonate with earlier observations made in bisulfite fluorescence cuvette experiments. Additionally, the amalgamated images from the green and red channels showcased evident color transitions, evolving prominently from a reddish-yellow hue to a discernible yellowish-green shade post-bisulfite exposure, as delineated in Fig. 11. Intriguingly, ratiometric images, computed by dividing the green channel values by those of the red channel, also underwent notable color alterations. These images shifted distinctly from a faint bluish-yellow to a subtle yellowish-blue shade upon bisulfite treatment, further accentuating the cellular response to the sulfur dioxide-inducing agent.

We utilized probe **A** to assess viscosity changes in first-instar *Drosophila melanogaster* larvae subjected to Monensin treatment. After pretreating these larvae with different Monensin concentrations (0 μM as the control, 20 μM, and 40 μM) for 4 h, we subsequently exposed them to a 2-h incubation period with 10 μM of probe **A** (Fig. 13). Our findings indicate a subtle fluorescence enhancement in the Monensin-treated larvae relative to the control group, suggesting a potential modulation of viscosity dynamics in response to the treatment. This observation underscores the utility of probe **A** in elucidating the cellular responses to Monensin-induced perturbations.

In summary, mitochondria stand as indispensable organelles central to eukaryotic cellular function, with roles transcending beyond mere ATP production to encompass pivotal cellular processes such as apoptosis, calcium signaling, and biosynthesis. Our investigation accentuates the emerging significance of intramitochondrial viscosity and sulfur dioxide (SO_2) levels as critical determinants of mitochondrial health and functionality. Notably, optimal mitochondrial viscosity emerges as a key regulator, influencing molecular diffusion, membrane dynamics, and essential biochemical reactions. The perturbations in viscosity have been intricately linked to a range of pathological conditions, including neurodegenerative diseases, diabetes, and cancer. Concurrently, the regulatory role of SO_2 within mitochondria, while paramount for energy modulation and oxidative stress responses, demands meticulous equilibrium, as imbalances precipitate cytotoxic effects leading to severe health complications. To address these burgeoning insights, our study introduces a dual-channel fluorescent probe, adeptly designed to facilitate real-time monitoring of mitochondrial viscosity and SO_2 levels within live cellular environments. Through strategic incorporation of electron-withdrawing acceptors within a coumarin dye matrix, this probe offers unprecedented capabilities, enabling ratiometric quantification of SO_2 devoid of interference from other reactive sulfur species. Moreover, its capacity for near-infrared fluorescence determination furnishes invaluable insights into mitochondrial viscosity dynamics, particularly in disease-relevant contexts. The application of this innovative probe, as evidenced in HeLa cells exposed to membrane-disrupting agents and immune activators, underscores its potential to elucidate the nuanced interplay of viscosity and SO_2 dynamics within mitochondria. By illuminating these critical facets, our methodology not only broadens the understanding of mitochondrial contributions to cellular energetics and redox homeostasis but also paves the way for groundbreaking therapeutic interventions targeting mitochondrial dysfunction. Moving forward, the insights gleaned from this research herald a promising era of exploration, offering novel avenues to address and mitigate disorders intricately tied to mitochondrial anomalies.

Author Statement

Our study introduces a dual-channel fluorescent probe capable of

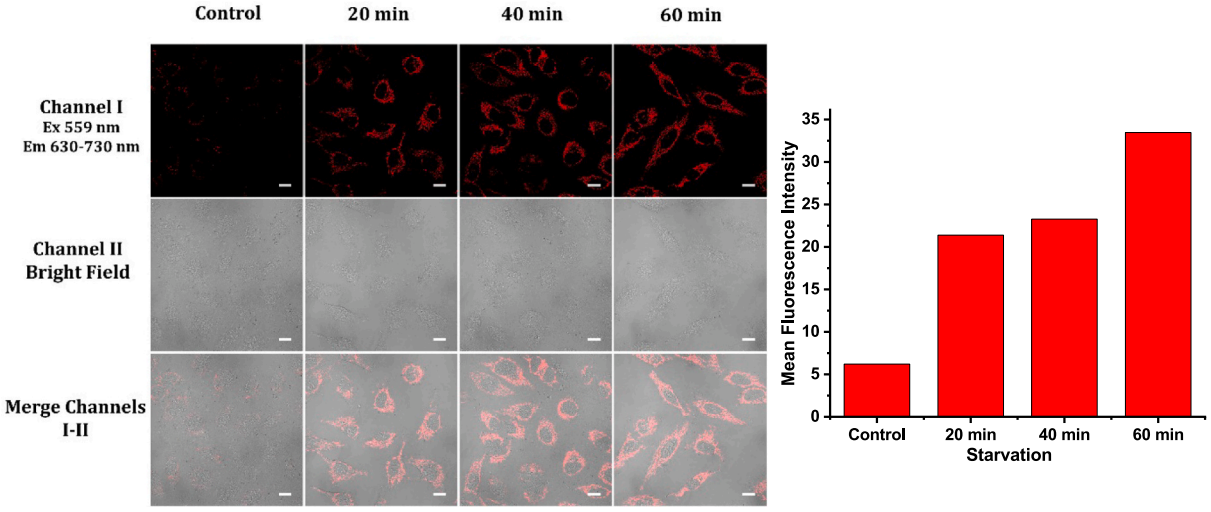

Fig. 11. Fluorescence microscopy images depicting HeLa cells treated with probe **A** (5 μM) in a serum-free fetal bovine medium over varying time intervals: 0, 20, 40, and 60 min. Fluorescence was captured within the 630–730 nm range using an excitation wavelength of 559 nm. Scale bars represent 50 μm. Histograms depicting the fluorescence intensity of probe **A** (5 μM) at various time intervals (right).

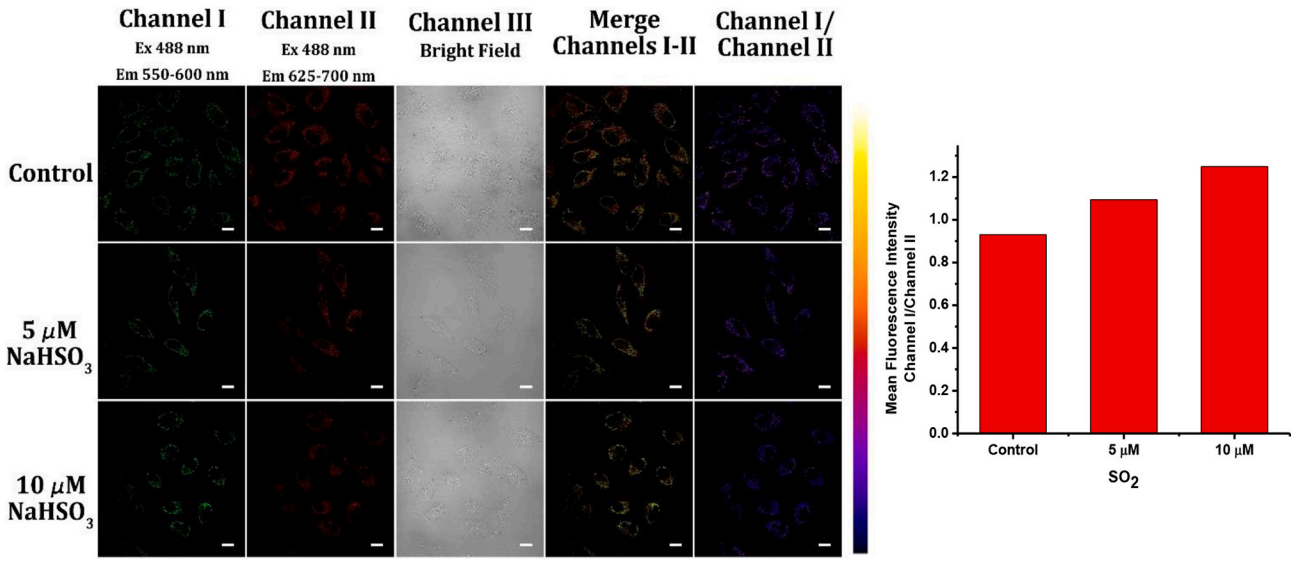

Fig. 12. Fluorescence microscopy images depicting HeLa cells treated with varying concentrations of $NaHSO_3$ (0 μM as control, 5 μM, and 10 μM) for 30 min, followed by an additional incubation with probe **A** (5 μM) for 20 min. Images captured in the green channel spanned a wavelength range of 550 to 600 nm, while those in the red channel ranged from 625 to 700 nm. Excitation for both channels was set at 488 nm. The scale bar denotes 50 μm. Histograms illustrating the fluorescence intensity of probe **A** (5 μM) at varying concentrations of $NaHSO_3$ (right). (For interpretation of the references to color in this figure legend, the reader is referred to the web version of this article.)

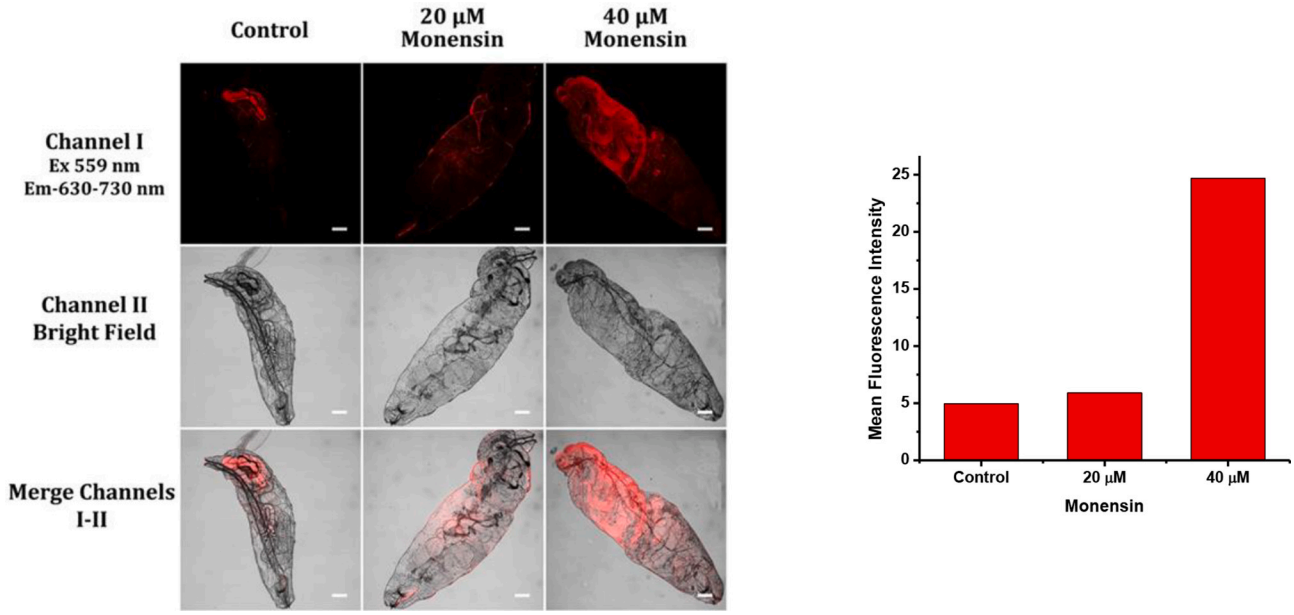

Fig. 13. Confocal fluorescence images depict first-instar *Drosophila melanogaster* larvae. These specimens underwent pretreatment with varying concentrations of Monensin (0 μM serving as the control, 20 μM, and 40 μM) for 4 h, followed by an incubation period of 2 h with 10 μM probe **A**. Imaging was conducted between 630 nm and 730 nm wavelengths, employing an excitation source at 559 nm. Histograms displaying the fluorescence intensity of probe **A** (10 μM) at varying concentrations of Monensin (right).

simultaneous monitoring of mitochondrial viscosity and sulfur dioxide (SO_2) levels within living cells. Leveraging the integration of electron-withdrawing acceptors into a coumarin dye matrix, our probe offers unparalleled precision in quantifying these crucial mitochondrial parameters. Notably, it distinguishes between distinct fluorescence peaks activated by SO_2, enabling interference-free ratiometric quantification. Furthermore, our probe facilitates near-infrared viscosity determination, particularly emphasizing mitochondrial dynamics. Through rigorous experimental validation and theoretical calculations, including Density Functional Theory (DFT) methods, we have established the efficacy and specificity of our probe. Moreover, our study demonstrates the utility of this innovative methodology in elucidating the impact of various cellular stimuli on mitochondrial viscosity dynamics. By shedding light on the intricate interplay between mitochondrial viscosity and SO_2 levels, our research opens new avenues for understanding cellular energetics, redox homeostasis, and the development of targeted interventions for mitochondrial-related disorders.

CRediT authorship contribution statement

Dilka Liyana Arachchige: Methodology, Formal analysis, Data curation. **Sushil K. Dwivedi:** Methodology, Investigation, Data

curation. **Adenike Mary Olowolagba:** Methodology, Investigation, Data curation. **Joseph Peters:** Investigation, Data curation. **Ashlyn Colleen Beatty:** Investigation, Data curation. **Alicia Guo:** Validation. **Crystal Wang:** Validation. **Thomas Werner:** Supervision, Investigation. **Rudy L. Luck:** Writing – review & editing, Writing – original draft, Supervision, Project administration, Funding acquisition. **Haiying Liu:** Writing – review & editing, Writing – original draft, Supervision, Project administration, Funding acquisition, Conceptualization.

Declaration of Competing Interest

The authors assert that they possess no recognized conflicting financial interests or personal connections that may have seemed to impact the work detailed in this paper.

Data availability

Data will be made available on request.

Acknowledgments

We acknowledge the computational resources provided by the high-performance computing infrastructure at Michigan Technological University for conducting crucial calculations on the probes. Furthermore, our heartfelt appreciation goes to the National Science Foundation for their invaluable assistance under award number 2117318, which facilitated the acquisition of a new NMR spectrometer. This equipment played an essential role in characterizing the chemical structures of the fluorescent probes. This research benefitted from generous support from the National Institute of General Medical Sciences, National Institutes of Health, under Award Numbers 2R15GM114751 and R15GM114751 for H. Liu, as well as R15GM152969-01 and R15 GM146206-01 for R. Luck and H. Liu.

Appendix A. Supplementary data

Supplementary data to this article can be found online at https://doi.org/10.1016/j.jphotobiol.2024.112986.

References

[1] P. Eyenga, B. Rey, L. Eyenga, S.S. Sheu, Regulation of oxidative phosphorylation of liver mitochondria in Sepsis, Cells 11 (10) (2022) 1598, https://doi.org/10.3390/cells11101598.

[2] S. Papa, P.L. Martino, G. Capitanio, A. Gaballo, D. De Rasmo, A. Signorile, V. Petruzzella, The oxidative phosphorylation system in mammalian mitochondria, in: R. Scatena, P. Bottoni, B. Giardina (Eds.), Advances in Mitochondrial Medicine, 2012, pp. 3–37.

[3] L. Chai, T.Y. Liang, Q. An, W. Hu, Y.Y. Wang, B.S. Wang, S.Z. Su, C.Y. Li, Near-infrared in and out: observation of autophagy during Strokevia a lysosome-targeting two-photon viscosity-dependent probe, Anal. Chem. 94 (15) (2022) 5797–5804, https://doi.org/10.1021/acs.analchem.1c05143.

[4] B.C. Chen, S.M. Mao, Y.Y. Sun, L.Y. Sun, N. Ding, C.D. Li, J. Zhou, A mitochondria-targeted near-infrared fluorescent probe for imaging viscosity in living cells and a diabetic mice model, Chem. Commun. 57 (36) (2021) 4376–4379, https://doi.org/10.1039/d1cc01104a.

[5] J.X. Hong, X.G. Guan, Y. Chen, X.D. Tan, S.Y. Zhang, G.Q. Feng, Mitochondrial membrane potential independent near-infrared mitochondrial viscosity probes for real-time tracking Mitophagy, Anal. Chem. 95 (13) (2023) 5687–5694, https://doi.org/10.1021/acs.analchem.2c05568.

[6] V. Juvekar, C.S. Lim, D.J. Lee, D.H. Song, C.K. Noh, H. Kang, S.J. Shin, H.M. Kim, Near-infrared Ratiometric two-photon probe for pH measurement in human stomach Cancer tissue, ACS Appl. Bio Mater. 4 (3) (2021) 2135–2141, https://doi.org/10.1021/acsabm.0c01546.

[7] P. Lei, M.L. Li, C. Dong, S.M. Shuang, Multifunctional mitochondria-targeting near-infrared fluorescent probe for viscosity, ONOO-, Mitophagy, and bioimaging, ACS Biomater Sci. Eng. 9 (6) (2023) 3581–3589, https://doi.org/10.1021/acsbiomaterials.3c00307.

[8] W.J. Shi, Y.F. Wei, J.R. Yang, H.Z. Li, Q.H. Wan, Y.X. Wang, H.X. Leng, K. Chen, J. W. Yan, Novel meso-trifluoromethyl BODIPY-based near-infrared-emitting fluorescent probes for organelle-specific imaging of cellular viscosity, Sensors Actuators B Chem. 359 (2022) 131594, https://doi.org/10.1016/j.snb.2022.131594.

[9] X.D. Wang, L. Fan, S.H. Wang, Y.W. Zhang, F. Li, Q. Zan, W.J. Lu, S.M. Shuang, C. Dong, Real-time monitoring mitochondrial viscosity during Mitophagy using a mitochondria-immobilized near-infrared aggregation-induced emission probe, Anal. Chem. 93 (6) (2021) 3241–3249, https://doi.org/10.1021/acs.analchem.0c04826.

[10] Y.F. Wei, X.F. Weng, X.L. Sha, R. Sun, Y.J. Xu, J.F. Ge, Simultaneous imaging of lysosomal and mitochondrial viscosity under different conditions using a NIR probe, Sensors Actuators B Chem. 326 (2021) 128954, https://doi.org/10.1016/j.snb.2020.128954.

[11] X. Wu, G.Y. Fu, Y. Li, S.J. Li, Q.Y. Zhao, F.P. Kong, L. Li, B. Tang, Dihydroxanthene-based near-infrared fluorescent probes for monitoring mitochondrial viscosity in living cells and mice, Anal. Chem. 95 (2023) 3544–3549, https://doi.org/10.1021/acs.analchem.2c05713.

[12] X. Wu, R.X. Zhang, Y. Li, Y.T. Gai, T.T. Feng, J.J. Kou, F.P. Kong, L. Li, B. Tang, Rational design of MMP-independent near-infrared fluorescent probes for accurately monitoring mitochondrial viscosity, Anal. Chem. 95 (19) (2023) 7611–7619, https://doi.org/10.1021/acs.analchem.3c00436.

[13] Y.C. Wu, C.X. Yin, W.J. Zhang, Y.B. Zhang, F.J. Huo, Mitochondrial-targeting near-infrared fluorescent probe for visualizing viscosity in drug-induced cells and a fatty liver mouse model, Anal. Chem. 94 (12) (2022) 5069–5074, https://doi.org/10.1021/acs.analchem.1c05288.

[14] X.Z. Yang, B. Xu, L. Shen, R. Sun, Y.J. Xu, Y.L. Song, J.F. Ge, Series of mitochondria/lysosomes self-targetable near-infrared Hemicyanine dyes for viscosity detection, Anal. Chem. 92 (5) (2020) 3517–3521, https://doi.org/10.1021/acs.analchem.0c00054.

[15] X.Y. Zhang, H.M. Yan, F.J. Huo, J.B. Chao, C.X. Yin, Dual-emission NIR fluorescent probe sensitive response biological microenvironment and sulfur dioxide, Sensors Actuators B Chem. 344 (2021) 130244, https://doi.org/10.1016/j.snb.2021.130244.

[16] Y.Y. Zhang, Z. Li, W. Hu, Z.H. Liu, A mitochondrial-targeting near-infrared fluorescent probe for visualizing and monitoring viscosity in live cells and Tissuese, Anal. Chem. 91 (15) (2019) 10302–10309, https://doi.org/10.1021/acs.analchem.9b02678.

[17] A.S. Zheng, H. Liu, X.N. Gao, K.H. Xu, B. Tang, A mitochondrial-targeting near-infrared fluorescent probe for revealing the effects of hydrogen peroxide and heavy metal ions on viscosity, Anal. Chem. 93 (26) (2021) 9244–9249, https://doi.org/10.1021/acs.analchem.1c01511.

[18] S.Y. Morita, Y. Ikeda, Regulation of membrane phospholipid biosynthesis in mammalian cells, Biochem. Pharmacol. 206 (2022) 115296, https://doi.org/10.1016/j.bcp.2022.115296.

[19] Q. Zhang, Y. Tamura, M. Roy, Y. Adachi, M. Iijima, H. Sesaki, Biosynthesis and roles of phospholipids in mitochondrial fusion, division and mitophagy, Cell. Mol. Life Sci. 71 (19) (2014) 3767–3778, https://doi.org/10.1007/s00018-014-1648-6.

[20] M.K. Goshisht, N. Tripathi, G.K. Patra, M. Chaskar, Organelle-targeting ratiometric fluorescent probes: design principles, detection mechanisms, bio-applications, and challenges, Chem. Sci. 14 (22) (2023) 5842–5871, https://doi.org/10.1039/d3sc01036h.

[21] X.D. Chen, Q. Chen, D. He, S.X. Yang, Y.F. Yang, J. Qian, L.L. Long, K. Wang, Mitochondria targeted and immobilized ratiometric NIR fluorescent probe for investigating SO2 phytotoxicity in plant mitochondria, Sensors Actuators B Chem. 370 (2022) 132433, https://doi.org/10.1016/j.snb.2022.132433.

[22] G.S. Fang, X.L. Yang, W.J. Wang, Y. Feng, W. Zhang, Y.L. Huang, C. Sun, M. Chen, X.M. Meng, Dual-detection of mitochondrial viscosity and SO2 derivatives with two cross-talk-free emissions employing a single two-photon fluorescent probe, Sensors Actuators B Chem. 297 (2019) 126777, https://doi.org/10.1016/j.snb.2019.126777.

[23] J.S. Lan, R.F. Zeng, Y. Ding, Y. Zhang, T. Zhang, T. Wu, A simple pyrene-hemicyanine fluorescent probe for colorimetric and ratiometric detection of SO2 derivatives in the mitochondria of living cells and zebrafish in vivo, Sensors Actuators B Chem. 268 (2018) 328–337, https://doi.org/10.1016/j.snb.2018.04.047.

[24] H.D. Li, X. Zhou, J.L. Fan, S. Long, J.J. Du, J.Y. Wang, X.J. Peng, Fluorescence imaging of SO2 derivatives in Daphnia magna with a mitochondria-targeted two-photon ratiometric fluorescent probe, Sensors Actuators B Chem. 254 (2018) 709–718, https://doi.org/10.1016/j.snb.2017.07.082.

[25] W.Y. Liu, D. Zhang, B.W. Ni, J. Li, H.B. Weng, Y. Ye, Mitochondria-targeted and FRET based ratiometric fluorescent probe for SO2 and its cell imaging, Sensors Actuators B Chem. 284 (2019) 330–336, https://doi.org/10.1016/j.snb.2018.12.158.

[26] Y. Liu, K. Li, M.Y. Wu, Y.H. Liu, Y.M. Xie, X.Q. Yu, A mitochondria-targeted colorimetric and ratiometric fluorescent probe for biological SO2 derivatives in living cells, Chem. Commun. 51 (50) (2015) 10236–10239, https://doi.org/10.1039/c5cc03055b.

[27] G.L. Song, A.K. Liu, H.L. Jiang, R.X. Ji, J. Dong, Y.Q. Ge, A FRET-based ratiometric fluorescent probe for detection of intrinsically generated SO2 derivatives in mitochondria, Anal. Chim. Acta 1053 (2019) 148–154, https://doi.org/10.1016/j.aca.2018.11.052.

[28] J.C. Xu, J. Pan, X.M. Jiang, C.Q. Qin, L.T. Zeng, H. Zhang, J.F. Zhang, A mitochondria-targeted ratiometric fluorescent probe for rapid, sensitive and specific detection of biological SO2 derivatives in living cells, Biosens. Bioelectron. 77 (2016) 725–732, https://doi.org/10.1016/j.bios.2015.10.049.

[29] J. Yang, K. Li, J.T. Hou, L.L. Li, C.Y. Lu, Y.M. Xie, X. Wang, X.Q. Yu, Novel tumor-specific and mitochondria-targeted near-infrared-emission fluorescent probe for SO2 derivatives in living cells, ACS Sens. 1 (2) (2016) 166–172, https://doi.org/10.1021/acssensors.5b00165.

[30] Y.T. Yang, T.T. Zhou, B.Z. Bai, C.X. Yin, W.Z. Xu, W. Li, Design of mitochondria-targeted colorimetric and ratiometric fluorescent probes for rapid detection of SO2 derivatives in living cells, Spectrochim Acta Part A Mol. Biomol. Spectrosc. 196 (2018) 215–221, https://doi.org/10.1016/j.saa.2018.01.066.
[31] D.S. Zhang, A.K. Liu, R.X. Ji, J. Dong, Y.Q. Ge, A mitochondria-targeted and FRET-based ratiometric fluorescent probe for detection of SO2 derivatives in water, Anal. Chim. Acta 1055 (2019) 133–139, https://doi.org/10.1016/j.aca.2018.12.042.
[32] M. Zhao, D.K. Liu, L. Zhou, B.Y. Wu, X.H. Tian, Q. Zhang, H.P. Zhou, J.X. Yang, J. Y. Wu, Y.P. Tian, Two water-soluble two-photon fluorescence probes for ratiometric imaging endogenous SO2 derivatives in mitochondria, Sensors Actuators B Chem. 255 (2018) 1228–1237, https://doi.org/10.1016/j.snb.2017.08.053.
[33] J.Y. Guo, B. Fang, H. Bai, L.M. Wang, B. Peng, X.J. Qin, L. Fu, C.H. Yao, L. Li, W. Huang, Dual/multi-responsive fluorogenic probes for multiple analytes in mitochondria: from design to applications, TrAC - Trends Anal. Chem. 155 (2022) 116697, https://doi.org/10.1016/j.trac.2022.116697.
[34] Y.F. Huang, J.P. Liang, Z.F. Fan, A review: small organic molecule dual/multi-organelle-targeted fluorescent probes, Talanta 259 (2023) 124529, https://doi.org/10.1016/j.talanta.2023.124529.
[35] C.G. Ma, W. Sun, L.M. Xu, Y. Qian, J.A. Dai, G.Y. Zhong, Y. Hou, J.L. Liu, B.X. Shen, A minireview of viscosity-sensitive fluorescent probes: design and biological applications, J. Mater. Chem. B 8 (42) (2020) 9642–9651, https://doi.org/10.1039/d0tb01146k.
[36] P. Ning, W.J. Wang, M. Chen, Y. Feng, X.M. Meng, Recent advances in mitochondria- and lysosomes-targeted small-molecule two-photon fluorescent probes, Chin. Chem. Lett. 28 (10) (2017) 1943–1951, https://doi.org/10.1016/j.cclet.2017.09.026.
[37] S. Zhang, H.Y. Zheng, L. Yang, Z.X. Li, M.M. Yu, NIR mitochondrial fluorescent probe for visualizing SO2/polarity in drug induced inflammatory mice, Anal. Chem. 95 (12) (2023) 5377–5383, https://doi.org/10.1021/acs.analchem.2c05737.
[38] W.Q. Chen, X.J. Liu, S. Chen, X.Z. Song, J. Kang, A real-time colorimetric and ratiometric fluorescent probe for rapid detection of SO₂ derivatives in living cells based on a near-infrared benzopyrylium dye, RSC Adv. 5 (32) (2015) 25409–25415, https://doi.org/10.1039/c4ra15067h.
[39] H. Crawford, M. Dimitriadi, J. Bassin, M.T. Cook, T.F. Abelha, J. Calvo-Castro, Mitochondrial targeting and imaging with small organic conjugated fluorophores: a review, Chem. Eur. J. 28 (72) (2022) e202202366, https://doi.org/10.1002/chem.202202366.
[40] M.T. Sun, T. Wang, X. Yang, H. Yu, S.H. Wang, D.J. Huang, Facile mitochondria localized fluorescent probe for viscosity detection in living cells, Talanta 225 (2021), https://doi.org/10.1016/j.talanta.2020.121996.
[41] D.X. Cao, Z.Q. Liu, P. Verwilst, S. Koo, P. Jangjili, J.S. Kim, W.Y. Lin, Coumarin-based small-molecule fluorescent Chemosensors, Chem. Rev. 119 (18) (2019) 10403–10519, https://doi.org/10.1021/acs.chemrev.9b00145.
[42] Y.F. Fan, Y. Wu, J. Hou, P. Wang, X.J. Peng, G.B. Ge, Coumarin-based near-infrared fluorogenic probes: recent advances, challenges and future perspectives, Coord. Chem. Rev. 480 (2023) 215020, https://doi.org/10.1016/j.ccr.2023.215020.
[43] Q.L. Sun, D.M. He, L.S. Zhang, Z.H. Li, L.B. Qu, Y.Q. Sun, Coumarin-hemicyanine-based far-red to near-infrared fluorescent probes: a new generation of fluorescent probe design platform, TrAC - Trends Anal. Chem. 167 (2023) 117272, https://doi.org/10.1016/j.trac.2023.117272.
[44] S. Xia, J.B. Wang, J.H. Bi, X. Wang, M.X. Fang, T. Phillips, A. May, N. Conner, M. Tanasova, F.T. Luo, H.Y. Liu, Fluorescent probes based on π-conjugation modulation between hemicyanine and coumarin moieties for ratiometric detection of pH changes in live cells with visible and near-infrared channels, Sensors Actuators B Chem. 265 (2018) 699–708, https://doi.org/10.1016/j.snb.2018.02.168.
[45] S. Xia, Y.B. Zhang, M.X. Fang, L. Mikesell, T.E. Steenwinkel, S.L. Wan, T. Phillips, R.L. Luck, T. Werner, H.Y. Liu, A FRET-based near-infrared fluorescent probe for Ratiometric detection of cysteine in mitochondria, ChemBioChem 20 (15) (2019) 1986–1994, https://doi.org/10.1002/cbic.201900071.
[46] Y.B. Zhang, S. Xia, S.L. Wan, T.E. Steenwinkel, T. Vohs, R.L. Luck, T. Werner, H. Y. Liu, Ratiometric detection of glutathione based on disulfide linkage rupture between a FRET Coumarin donor and a rhodamine acceptor, ChemBioChem 22 (13) (2021) 2282–2291, https://doi.org/10.1002/cbic.202100108.
[47] Y.B. Zhang, Y.N. Yan, S. Xia, S.L. Wan, T.E. Steenwinkel, J. Medford, E. Durocher, R.L. Luck, T. Werner, H.Y. Liu, Cell membrane-specific fluorescent probe featuring dual and aggregation-induced emissions, ACS Appl. Mater. Interfaces 12 (18) (2020) 20172–20179, https://doi.org/10.1021/acsami.0c00903.
[48] S.K. Dwivedi, D.L. Arachchige, T. Vohs, J. Tang, K. Usimaki, A.M. Olowolagba, D. R. Fritz, R.L. Luck, T. Werner, H. Liu, Near-infrared rhodol dyes bearing salicylaldehyde moieties for ratiometric pH sensing in live cells during mitophagy and under hypoxia conditions, J. Mater. Chem. B 11 (13) (2023) 2852–2861, https://doi.org/10.1039/d2tb02791g.
[49] C.F. Macrae, I.J. Bruno, J.A. Chisholm, P.R. Edgington, P. McCabe, E. Pidcock, L. Rodriguez-Monge, R. Taylor, J. van de Streek, P.A. Wood, Mercury CSD 2.0 - new features for the visualization and investigation of crystal structures, J. Appl. Crystallogr. 41 (2008) 466–470.
[50] D.L. Arachchige, S.K. Dwivedi, M. Waters, S. Jaeger, J. Peters, D.R. Tucker, M. Geborkoff, T. Werner, R.L. Luck, B. Godugu, H.Y. Liu, Sensitive monitoring of NAD(P)H levels within cancer cells using mitochondria-targeted near-infrared cyanine dyes with optimized electron-withdrawing acceptors, J. Mater. Chem. B 12 (2) (2024) 448–465, https://doi.org/10.1039/d3tb02124f.
[51] S.K. Dwivedi, D.L. Arachchige, A. Olowolagba, M. Mahmoud, J. Cunnien, D. R. Tucker, D. Fritz, T. Werner, R.L. Luck, H.Y. Liu, Thiophene-based organic dye with large stokes shift and deep red emission for live cell NAD(P)H detection under varying chemical stimuli, J. Mater. Chem. B 11 (27) (2023) 6296–6307, https://doi.org/10.1039/d3tb00645j.
[52] S.K. Dwivedi, D.L. Arachchige, M. Waters, S. Jaeger, M. Mahmoud, A. M. Olowolagba, D.R. Tucker, M.R. Geborkoff, T. Werner, R.L. Luck, B. Godugu, H. Y. Liu, Near-infrared absorption and emission probes with optimal connection bridges for live monitoring of NAD(P)H dynamics in living systems, Sensors Actuators B Chem. 402 (2024) 135073, https://doi.org/10.1016/j.snb.2023.135073.
[53] Y.B. Zhang, D.L. Arachchige, A. Olowolagba, R.L. Luck, H.Y. Liu, Near-infrared fluorescent probe based on rhodamine derivative for detection of NADH in live cells, Methods 204 (2022) 22–28, https://doi.org/10.1016/j.ymeth.2022.03.019.
[54] S. Park, W.H. Jung, M. Pittman, J.J. Chen, Y. Chen, The effects of stiffness, fluid viscosity, and geometry of microenvironment in homeostasis, aging, and diseases: a brief review, J. Biomech. Eng. 142 (10) (2020) 100804, https://doi.org/10.1115/1.4048110.
[55] M.W. Rampling, Haemorheological disturbances in hypertension: the influence of diabetes and smoking, Clin. Hemorheol. Microcirc. 21 (3–4) (1999) 183–187.
[56] M.M. Smith, P.C.Y. Chen, C.S. Li, S. Ramanujam, A.T.W. Cheung, Whole blood viscosity and microvascular abnormalities in Alzheimer's disease, Clin. Hemorheol. Microcirc. 41 (4) (2009) 229–239, https://doi.org/10.3233/ch-2009-1174.
[57] F.Y. Tang, K. Wang, X.L. Liu, X.L. Zhang, W.T. Zhou, Z.G. Mu, T. Zhang, W. Shu, Y. Y. Liu, H.B. Xiao, Small molecular fluorescent probes for Alzheimer's disease associated active species, Chem. Eur. J. 29 (35) (2023) e202300592, https://doi.org/10.1002/chem.202300592.
[58] H.D. Chapman, T.K. Jeffers, R.B. Williams, Forty years of monensin for the control of coccidiosis in poultry, Poult. Sci. 89 (9) (2010) 1788–1801, https://doi.org/10.3382/ps.2010-00931.
[59] L.M.E. Mammi, M. Guadagnini, G. Mechor, J.M. Cainzos, I. Fusaro, A. Palmonari, A. Formigoni, The use of Monensin for ketosis prevention in dairy cows during the transition period: a systematic review, Animals 11 (7) (2021) 1988, https://doi.org/10.3390/ani11071988.
[60] V. Rajendran, H.S. Ilamathi, S. Dutt, T.S. Lakshminarayana, P.C. Ghoshi, Chemotherapeutic potential of Monensin as an anti-microbial agent, Curr. Top. Med. Chem. 18 (22) (2018) 1976–1986, https://doi.org/10.2174/1568026619666181129141151.
[61] M.R.R. Ahvanooei, M.A. Norouzian, A.H. Piray, P. Vahmani, M.H. Ghaffari, Effects of monensin supplementation on lactation performance of dairy cows: a systematic review and dose-response meta-analysis, Sci. Rep. 13 (1) (2023), https://doi.org/10.1038/s41598-023-27395-9.
[62] X. Wang, X.Y. Wu, Z.L. Zhang, C. Ma, T.T. Wu, S.L. Tang, Z.Y. Zeng, S.F. Huang, C. Gong, C.F. Yuan, L.H. Zhang, Y.X. Feng, B. Huang, W. Liu, B. Zhang, Y. Shen, W. P. Luo, X. Wang, B. Liu, Y. Lei, Z.Y. Ye, L. Zhao, D.G. Cao, L.J. Yang, X. Chen, R. C. Haydon, H.H. Luu, B. Peng, X.B. Liu, T.C. He, Monensin inhibits cell proliferation and tumor growth of chemo-resistant pancreatic cancer cells by targeting the EGFR signaling pathway, Sci. Rep. 8 (2018), https://doi.org/10.1038/s41598-018-36214-5.
[63] M. Vraila, E. Asp, F.R. Melo, M. Grujic, O. Rollman, G. Pejler, M. Lampinen, Monensin induces secretory granule-mediated cell death in eosinophils, J. Allergy Clin. Immunol. 152 (5) (2023), https://doi.org/10.1016/j.jaci.2023.07.012.
[64] M. Caroff, D. Karibian, Structure of bacterial lipopolysaccharides, Carbohydr. Res. 338 (23) (2003) 2431–2447, https://doi.org/10.1016/j.carres.2003.07.010.
[65] B.O. Nilsson, Mechanisms involved in regulation of periodontal ligament cell production of pro-inflammatory cytokines: implications in periodontitis, J. Periodontal Res. 56 (2) (2021) 249–255, https://doi.org/10.1111/jre.12823.
[66] M.C. Pardon, Lipopolysaccharide hyporesponsiveness: protective or damaging response to the brain? Romanian J. Morphol. Embryol. 56 (3) (2015) 903–913.
[67] Y. Wang, N. Liu, B.W. Lu, Mechanisms and roles of mitophagy in neurodegenerative diseases, CNS Neurosci. Ther. 25 (7) (2019) 859–875, https://doi.org/10.1111/cns.13140.
[68] M. Redmann, M. Dodson, M. Boyer-Guittaut, V. Darley-Usmar, J.H. Zhang, Mitophagy mechanisms and role in human diseases, Int. J. Biochem. Cell Biol. 53 (2014) 127–133, https://doi.org/10.1016/j.biocel.2014.05.010.
[69] S.K. Dwivedi, D.L. Arachchige, T. Vohs, J.N. Tang, K. Usimaki, A.M. Olowolagba, D.R. Fritz, R.L. Luck, T. Werner, H.Y. Liu, Near-infrared rhodol dyes bearing salicylaldehyde moieties for ratiometric pH sensing in live cells during mitophagy and under hypoxia conditions, J. Mater. Chem. B 11 (13) (2023) 2852–2861, https://doi.org/10.1039/d2tb02791g.
[70] S.A. Xia, J.B. Wang, Y.B. Zhang, N. Whisman, J.H. Bi, T.E. Steenwinkel, S.L. Wan, J. Medford, M. Tajiri, R.L. Luck, T. Werner, H.Y. Liu, Ratiometric fluorescent probes based on through-bond energy transfer of cyanine donors to near-infrared hemicyanine acceptors for mitochondrial pH detection and monitoring of mitophagy, J. Mater. Chem. B 8 (8) (2020) 1603–1615, https://doi.org/10.1039/c9tb02302j.
[71] Y.B. Zhang, S. Xia, L. Mikesell, N. Whisman, M.X. Fang, T.E. Steenwinkel, K. Chen, R.L. Luck, T. Werner, H.Y. Liu, Near-infrared hybrid Rhodol dyes with Spiropyran switches for sensitive Ratiometric sensing of pH changes in mitochondria and Drosophila melanogaster first-instar larvae, ACS Appl. Bio Mater. 2 (11) (2019) 4986–4997, https://doi.org/10.1021/acsabm.9b00710.